

Combination of dissipative and dispersive coupling in the cavity optomechanical systems

Alexandr Karpenko ¹ and Sergey P. Vyatchanin ^{1,2}

¹*Faculty of Physics, M.V. Lomonosov Moscow State University, Leninskie Gory, Moscow 119991, Russia*

²*Quantum Technology Centre, M.V. Lomonosov Moscow State University, Leninskie Gory, Moscow 119991, Russia*



(Received 2 February 2022; accepted 13 May 2022; published 6 June 2022)

An analysis is given for the Fabry-Perot cavity having a combination of dissipative and dispersive optomechanical coupling. It is established that the combined coupling leads to optical rigidity. At the same time, this rigidity appears in systems with the combined coupling on the resonant pump, which is not typical for pure dispersive and dissipative couplings. A proposal is made to use this system to detect small signal forces with better sensitivity than the standard quantum limit. It is also demonstrated that this optomechanical system can create ponderomotive squeezing with controllable parameters over a wider range than ponderomotive squeezing using dispersive coupling.

DOI: [10.1103/PhysRevA.105.063506](https://doi.org/10.1103/PhysRevA.105.063506)

I. INTRODUCTION

Optomechanics is studying the fundamental sensitivity limitations in measuring the position of test mass. This sensitivity can be very high. For example, a relative mechanical displacement detected can be smaller than the size of a proton. This feature is widely used in gravitational wave detectors [1–6], in magnetometers [7,8], and in torque sensors [9–11].

The fundamental limitation is provided by the quantum noise. In a conventional scheme of a resonantly pumped Fabry-Perot (FP) cavity with a movable end mirror (the test mass), the phase of light, reflected from the cavity, contains information on the position of the test mass. The limit sensitivity is restricted by the well-known standard quantum limit (SQL) [12,13], which is an interplay between phase fluctuations of incident light (the measurement of error) and the Lebedev' fluctuation light pressure force (backaction).

The SQL has been investigated in many systems ranging from macroscopic kilometer-size gravitational wave detectors [14] to microcavities [15,16]. Detecting classical force acting on a test mass in optomechanical systems is an example of measurements restricted by the SQL. It can be surpassed by applying a variational measurement [14,17,18], squeezed light input [19–25], optomechanical speed measurement [26,27], or optical spring [28,29]. The SQL can be also be avoided using coherent quantum noise cancellation [30–32].

There are two types of optomechanical coupling, namely, dispersive and dissipative coupling. In dispersive coupling, displacing the mirror changes the normal cavity frequency, whereas in dissipative coupling displacing the test mass brings about a change in the input mirror transmittance, altering, thereby, the cavity relaxation rate. Dissipative coupling was proposed theoretically [33] and confirmed experimentally [9,34–36] about a decade ago. This phenomenon has been investigated in numerous optomechanical systems, including the FP interferometer [9,34–36], the Michelson-Sagnac interferometer [37–42], and ring resonators [43,44]. It has been demonstrated that an optomechanical transducer based on dissipative coupling allows realizing a

quantum speed meter which, in turn, helps to avoid the SQL [40].

The natural question is to what extent the *combination* of dispersive and dissipative coupling can improve the sensitivity of an optomechanical system to detect the signal of the displaced test mass. It is known that squeezing output quadratures is dramatically different for purely dispersive and dissipative coupling [9,37–40,42]. Seemingly, their combination does not look promising, but this conclusion is not correct.

In this paper we analyze a FP cavity featuring a combination of these different types of coupling and demonstrate that the SQL can be surpassed. The physical reason is the optical rigidity formed by the combination of both dispersive and dissipative coupling. We also demonstrate that this combined coupling gives the possibility to obtain ponderomotive-frequency-dependent squeezing with controllable parameters over a wider range compared with ponderomotive squeezing using dispersive coupling. Such frequency-dependent squeezing can be used in laser gravitational wave antennas.

II. MODEL

We consider one-dimensional FP cavity. Its optical mode with the eigenfrequency ω_0 is pumped using resonant light (the pump frequency $\omega_p = \omega_0$). The optical mode is coupled with the mechanical system represented by the free mass m . The eigenfrequency ω of the cavity and the relaxation rate γ of the optical mode depend on the test mass displacement y . Signal F_s acts on the free mass, changing its position.

For the description of this system, we use the input-output formalism (see Chap. 7 in Ref. [45]). The Hamiltonian of the system can be expressed as

$$\hat{H} = \hbar\omega_0(1 + \xi\hat{y})\hat{a}_c^\dagger\hat{a}_c + \frac{\hat{p}^2}{2m} + \hat{H}_\gamma + \hat{H}_T - F_s\hat{y}, \quad (2.1a)$$

$$\hat{H}_T = \int_0^\infty \hbar\omega \hat{b}_\omega^\dagger \hat{b}_\omega \frac{d\omega}{2\pi}, \quad (2.1b)$$

$$\hat{H}_\gamma = -i\hbar\sqrt{\gamma} \int_0^\infty (\hat{b}_\omega \hat{a}_c^\dagger - \hat{a}_c \hat{b}_\omega^\dagger) \frac{d\omega}{2\pi}, \quad (2.1c)$$

$$\gamma = \gamma_0(1 + \eta\hat{y}), \quad \sqrt{\gamma} \simeq \sqrt{\gamma_0} \left(1 + \frac{\eta}{2}\hat{y}\right). \quad (2.1d)$$

Here \hat{p} is the momentum of the test mass, \hat{a}_c and \hat{a}_c^\dagger are annihilation and creation operators describing the intracavity optical field, \hat{H}_T is the Hamiltonian of the electromagnetic field outside the cavity (thermal bath and pump), \hat{H}_γ describes coupling between intracavity and extracavity optical fields,¹ and ξ and η are the coefficients of dispersive and dissipative coupling, respectively.

From the Hamiltonian Eqs. (2.1) we obtain a set of quantum stochastic differential Eqs. (A1) describing the time evolution of the optomechanical system. A detailed solution of these equations is presented in Appendix A. Here we analyze the solutions obtained.

When solving the equations, we used the approximation of slow amplitudes Eq. (A2). Below we express these amplitudes as large constant amplitudes (denoted by capital letters) plus small amplitudes (denoted by the same letters in lowercase) to describe the noise and signal components:

$$\hat{a}_c = A_0 + \hat{a}_0, \quad \hat{a}_{\text{in}} = A + \hat{a}, \quad \hat{a}_{\text{out}} = A_1 + \hat{a}_1, \quad (2.2)$$

where \hat{a}_{in} and \hat{a}_{out} are the input and output fields, respectively.

Here and below we assume that the input wave is in a coherent state, so operator \hat{a} describes the vacuum fluctuation wave having the following commutator and correlator:

$$[\hat{a}(t), \hat{a}^\dagger(t')] = \delta(t - t'), \quad \langle \hat{a}(t) \hat{a}^\dagger(t') \rangle = \delta(t - t'). \quad (2.3)$$

Since we are interested in the spectral characteristics of small fluctuations, we proceed to the Fourier representation. The Fourier transform can be defined as follows:

$$\hat{a}(t) = \int_{-\infty}^{\infty} a(\Omega) e^{-i\Omega t} \frac{d\Omega}{2\pi}, \quad (2.4)$$

and similarly for other values denoting the Fourier transform by the same letter without a hat. One can derive the analog of Eq. (2.3) for the Fourier transform of the input fluctuation operators:

$$[a(\Omega), a^\dagger(\Omega')] = 2\pi \delta(\Omega - \Omega'), \quad (2.5)$$

$$\langle a(\Omega) a^\dagger(\Omega') \rangle = 2\pi \delta(\Omega - \Omega'). \quad (2.6)$$

Because the radiation pressure in the optical cavities produces ponderomotive squeezing, we find it convenient to think about the fields not in terms of the single-photon modes, whose annihilation operators are $a(\Omega)$, but rather in terms of the correlated two-photon modes whose field amplitudes are

$$a_a = \frac{a(\Omega) + a^\dagger(-\Omega)}{\sqrt{2}}, \quad a_\phi = \frac{a(\Omega) - a^\dagger(-\Omega)}{i\sqrt{2}}. \quad (2.7)$$

¹The Hamiltonian of coupling \hat{H}_γ is an approximation we need to get a Markov quantum stochastic process.

We can easily obtain the phase and amplitude quadratures of the output and internal fields from Eqs. (A11) as follows:

$$a_{1a} = \frac{\frac{\gamma_0}{2} + i\Omega}{\frac{\gamma_0}{2} - i\Omega} a_a - \frac{i\Omega\eta A}{\frac{\gamma_0}{2} - i\Omega} \sqrt{2}y_\Omega, \quad (2.8a)$$

$$a_{1\phi} = \frac{\frac{\gamma_0}{2} + i\Omega}{\frac{\gamma_0}{2} - i\Omega} a_\phi - \frac{2\omega_0\xi A}{\frac{\gamma_0}{2} - i\Omega} \sqrt{2}y_\Omega, \quad (2.8b)$$

$$a_{0a} = \frac{\sqrt{\gamma_0}}{\frac{\gamma_0}{2} - i\Omega} a_a - \frac{\sqrt{\gamma_0}\eta A}{\sqrt{2}\left(\frac{\gamma_0}{2} - i\Omega\right)} y_\Omega, \quad (2.8c)$$

$$a_{0\phi} = \frac{\sqrt{\gamma_0}}{\frac{\gamma_0}{2} - i\Omega} a_\phi - \frac{2\omega_0\xi A}{\sqrt{\gamma_0}\left(\frac{\gamma_0}{2} - i\Omega\right)} \sqrt{2}y_\Omega, \quad (2.8d)$$

$$y_\Omega = -\frac{F_\Omega}{m\Omega^2} + \frac{2\sqrt{2}\hbar\omega_0\xi A}{\sqrt{\gamma_0}m\Omega^2} a_{0a} + \frac{\sqrt{\gamma_0}\eta\hbar A}{\sqrt{2}m\Omega^2} \left(\frac{2}{\sqrt{\gamma_0}} a_\phi - a_{0\phi}\right). \quad (2.8e)$$

Here y_Ω and F_Ω are the Fourier transforms of the displacement y and the signal F_s , respectively.

From Eqs. (2.8) we see that the amplitude quadrature of the output field provides information about the speed of the probe mass $-i\Omega y_\Omega$, which corresponds to the dissipative coupling. In contrast, the phase quadrature provides information about the displacement of the probe mass, which is typical for the dispersive coupling.

Let us substitute Eqs. (2.8c) and (2.8d) into the equation for the spectrum of the displacement y Eq. (2.8e):

$$(K - m\Omega^2)y_\Omega = F_\Omega + F_\Pi, \quad (2.9a)$$

$$F_\Pi = -\frac{2\sqrt{2}\hbar\omega_0\xi A}{\frac{\gamma_0}{2} - i\Omega} a_a - i\frac{\sqrt{2}\hbar\Omega\eta A}{\frac{\gamma_0}{2} - i\Omega} a_\phi, \quad (2.9b)$$

$$K(\Omega) = -\frac{4\hbar\omega_0\xi\eta A^2}{\frac{\gamma_0}{2} - i\Omega} \simeq \kappa - i\Omega\delta, \quad (2.9c)$$

$$\kappa = -\frac{8\hbar\omega_0\xi\eta A^2}{\gamma_0}, \quad \delta = \frac{16\hbar\omega_0\xi\eta A^2}{\gamma_0^2}. \quad (2.9d)$$

Here F_Π is the fluctuation backaction force, and $K(\Omega)$ is the optical rigidity which is associated with both dissipative and dispersive coupling ($K \sim \xi\eta$). Note that this rigidity appears at the resonance pump. Recall, in cases of pure dispersive [46] or pure dissipative [41] coupling, optical rigidity is possible only in the *detuned* pump.

We expand rigidity Eq. (2.9c) into the Taylor series over $i\Omega$ keeping only the two first terms [below we assume $\gamma_0 \gg \Omega$ Eq. (4.2)]. This optical rigidity is unstable. If κ is positive then the mechanical viscosity δ introduced is negative and vice versa. The rigidity κ is positive when $\xi\eta < 0$. When κ is positive, the probe mass effectively acts as a harmonic oscillator which is affected by the signal F_s and the fluctuation backaction force.

In Ref. [42] we considered a similar system with combined coupling, but without a cavity, the main difference of which, as compared with the cavity case, is the possibility to measure quadratures in *two* output ports, whereas in the cavity case, considered here, we have only *one* output port. In spite of this restriction we found for the cavity case the

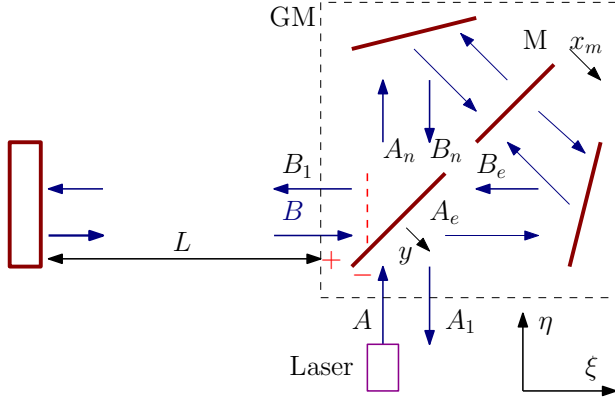


FIG. 1. Michelson-Sagnac interferometer as a generalized mirror (GM) of the FP cavity. Combined coupling takes place when the beam splitter is movable but the mirror M ($x_m = \text{const}$) is fixed.

best combination of quadratures of the output field in order to measure the signal force with sensitivity better than that of the SQL. Optical rigidity also appeared in systems without a cavity, but it did not depend on frequency, unlike the system under consideration. This is due to the fact that the field in the cavity is not set instantly, but with some delay, and the optical rigidity is set with a delay. Because of this, the optical rigidity in a system with a cavity depends on the frequency.

III. EXAMPLES OF REALIZATIONS OF COMBINED COUPLING

For a realization of the combination of dissipative and dispersive couplings we use the Michelson-Sagnac interferometer (MSI) as one of the mirrors in the FP cavity (see Fig. 1). The MSI consists of the 50/50 beam splitter (BS) and three completely reflecting mirrors. This interferometer can be considered as a generalized mirror having amplitude transmittance T and reflectivity R depending on the displacements z_m of the mirror M and y_{BS} of the BS. So input-output relations have the following forms (see notation on Fig. 1):

$$A_1 = BT + e^{-ik\sqrt{2}y}AR, \quad (3.1a)$$

$$B_1 = AT - e^{ik\sqrt{2}y}BR, \quad (3.1b)$$

$$R = \cos k(2z_m + \sqrt{2}y), \quad (3.1c)$$

$$T = \sin k(2z_m + \sqrt{2}y), \quad (3.1d)$$

where \mathcal{A} and \mathcal{B} are amplitudes of coherent monochromatic fields, and $k = \frac{\omega}{c}$ is the wave vector.

A detailed analysis of the MSI is given in Refs. [37–42]. We assume that the waves passing through the BS acquire a phase shift equal to $\frac{\pi}{2}$, and the phases of the waves reflected from the BS are determined only by the displacement of the BS itself. We also assume that the spectral frequencies Ω , characterizing the displacements of the BS and the moving mirror M , are small enough: $\Omega t_{\text{in}} \ll 1$, where t_{in} is the round-trip time of light between the BS and the mirror M . This means that the circulating fields change phase almost instantly at small displacements of the BS and the mirror M . The amplitude transmittance T and the reflectivity R of the generalized mirror depend only on positions z_m and y .

Below we can designate displacement as

$$y \Rightarrow y_0 + y, \quad z_m \Rightarrow z_0 + z, \quad (3.2)$$

where z_0 and y_0 are the mean constants (to be chosen) and z and y are small variables.

Below we consider only the situation of a movable beam splitter and the mirror M is fixed (that is $z = 0$). Then we can expand R and T (3.1) into the following series:

$$\begin{aligned} R &\simeq R_0 - T_0 k\sqrt{2}y, \\ T &\simeq T_0 + R_0 k\sqrt{2}y, \end{aligned} \quad (3.3a)$$

$$\begin{aligned} R_0 &= \cos k(2z_0 + \sqrt{2}y_0), \\ T_0 &= \sin k(2z_0 + \sqrt{2}y_0), \end{aligned} \quad (3.3b)$$

For simplicity we put $y_0 = 0$ below, and then only z_0 defines T_0 and R_0 .

The MSI is a part of the FP cavity. The field B_1 propagates to the end mirror (we consider that it is completely reflecting), reflects, and comes back to the beam splitter. In the stationary mode, the operation fields B and B_1 have the following coupling:

$$B = B_1 e^{i2kL}, \quad (3.4)$$

where L is the distance between the beam splitter and the end mirror.

Let us substitute Eq. (3.4) in Eqs. (3.1):

$$A_1 = B_1 e^{i2kL} T + e^{-ik\sqrt{2}y} A R, \quad (3.5a)$$

$$B_1 = A T - e^{ik\sqrt{2}y} B_1 e^{i2kL} R. \quad (3.5b)$$

The internal field's power I_0 is given by the ratio

$$I_0 = \frac{T^2 I}{1 + R^2 + 2R \cos 2k(L + \frac{y}{\sqrt{2}})}, \quad (3.6)$$

where I is the input field power.

This power achieves a maximum of $e^{2ik(L+y/\sqrt{2})} = -1$ (here and below we assume that $R > 0$). We can find the resonant frequency from the following equation:

$$w_r = \frac{\omega_0}{1 + \frac{y}{\sqrt{2}L}} \simeq \omega_0 \left(1 - \frac{y}{\sqrt{2}L} \right). \quad (3.7)$$

Here ω_0 is the resonant frequency by $y = 0$.

Now let us find the half bandwidths of the cavity γ_0 . Let us assume that the wave vector k in Eq. (3.6) is equal to $(\omega_r + \gamma)/c$ ($\omega_r \gg \gamma$) so that $I_0 = I_{0\text{max}}/2$. Then we get the following relation for γ :

$$\gamma = \frac{2(1-R)}{\tau\sqrt{R}} \simeq \frac{T^2}{\tau} \simeq \frac{T_0^2}{\tau} \left(1 + \frac{2\sqrt{2}k_0 R_0}{T_0} \right). \quad (3.8)$$

Here we consider that $T_0 \ll 1$.

Let us compare Eqs. (3.7) and (3.8) with Eqs. (2.1). We see that coefficients of dispersive (ξ) and dissipative (η) coupling for the system described above have the following forms:

$$\gamma_0 = \frac{T_0^2}{\tau}, \quad \xi = -\frac{1}{\sqrt{2}L}, \quad \eta = \frac{2\sqrt{2}k_0}{T_0}. \quad (3.9)$$

In Table I we list parameters of the system described above, which can be used in a laboratory experiment, for example,

TABLE I. Parameters of the optomechanical system.

Parameter	Value
Medium amplitude transmittance of MSI T_0	0.01
Probe mass m	50 g
Pump frequency $\omega_0/2\pi$	300 THz
Pump power I_0	42 mW
Cavity length L	1 m
Cavity half bandwidth γ_0	15 000 s ⁻¹
Coefficient of the dissipative coupling η	1.78×10^9 m ⁻¹
Coefficient of the dispersive coupling ξ	-0.71 m ⁻¹

for the creation of a frequency-dependent squeezed vacuum to inject it into the dark port of laser gravitational wave detectors (LIGO, Virgo)—see some details in Sec. V below.

Another example of realizing combined coupling is given in Ref. [39]. The authors describe an optical-mechanical system similar to the one presented above, but the test mass is a partially transmitting mirror, M, and the beam splitter is immobile (see Fig. 1). For this case the input-output relations can be written as follows:

$$\mathcal{A}_1 = i\mathcal{B}\mathbb{T} + \mathcal{A}\mathbb{R}_{\triangleright}, \quad (3.10a)$$

$$\mathcal{B}_1 = i\mathcal{A}\mathbb{T} + \mathcal{B}\mathbb{R}_{\triangleleft}, \quad (3.10b)$$

$$\mathbb{T} = e^{ikl_+} r_M \sin 2k\delta l, \quad (3.10c)$$

$$\mathbb{R}_{\triangleright} = e^{ikl_+} (r_M \cos 2k\delta l - it_M), \quad (3.10d)$$

$$\mathbb{R}_{\triangleleft} = e^{ikl_+} (r_M \cos 2k\delta l + it_M). \quad (3.10e)$$

Here r_M and t_M are the amplitude reflectivity and transmittance of the mirror, l_+ and δl are the sum and the difference of the lengths of the MSI arms, respectively. We consider that $\delta l = z_0 + z$, where z_0 is a constant and z is a small displacement, $kz \ll 1$.

Now we can find the coefficients of dispersive ξ_1 and dissipative η_1 coupling for this optomechanical system by conducting the analysis presented above. They are as follows:

$$\gamma_1 = \frac{r_M^2 T_1^2}{\tau}, \quad \xi_1 = -\frac{T_1 t_M r_M}{L}, \quad \eta_1 = \frac{4k_0}{T_1}. \quad (3.11)$$

Here we assume that $|T_1| = |\sin 2kz_0| \ll 1$ and we find the resonant frequency ω_0 from $e^{ik(2L+l_+)+i\phi_0} = 1$, where $\phi_0 = \arctan(t_M/r_M)$.

These examples show that we can choose coupling coefficients ξ and η within some bounds.

IV. DETECTING SIGNAL FORCE

We consider an optomechanical system with a combination of both couplings ξ and η as a signal force detector, assuming that ξ and η can be varied *arbitrary*. Let us find the sensitivity of this measurement.

We assume that quadratures of the output field, Eqs. (2.8a) and (2.8b), are processed optimally for this purpose. Let us

substitute (2.9) in equations of quadratures Eqs. (2.8a) and (2.8b):

$$a_{1a} = \frac{(x_0^2 - x^2)a_a - P_m x^2 a_\phi - ix^2 \sqrt{2P_m} f_s}{(x_0^2 - x^2) - ix\delta_m}, \quad (4.1a)$$

$$a_{1\phi} = \frac{(x_0^2 - x^2)a_\phi + Q_m D^2 a_a - xD\sqrt{2Q_m} f_s}{(x_0^2 - x^2) - ix\delta_m}, \quad (4.1b)$$

$$P_m = \frac{8\hbar\eta^2 A^2}{m\gamma_0^2}, \quad Q_m = \frac{32\hbar\xi^2 A^2}{m\gamma_0^2}, \quad (4.1c)$$

$$\delta_m = \frac{\delta}{m\gamma_0} = D\sqrt{P_m Q_m}, \quad x = \frac{\Omega}{\gamma_0}, \quad x_0 = \frac{\Omega_0}{\gamma_0},$$

$$\Omega_0 = \sqrt{\frac{\kappa}{m}}, \quad f_s = \frac{F_\Omega}{\sqrt{2\hbar m \Omega^2}}, \quad D = \frac{\omega_0}{\gamma_0}. \quad (4.1d)$$

Here f_s is the signal force normalized to the SQL, κ and δ are given by Eq. (2.9d), Ω_0 is the resonant frequency which appears due to the optical rigidity Eq. (2.9d), and D is the quality factor of the optical cavity. Here and below we assume that $\xi\eta = -|\xi\eta|$ and

$$\Omega, \Omega_0 \ll \gamma_0, \quad \text{or} \quad x, x_0 \ll 1. \quad (4.2)$$

Recall, in the case of pure dissipative coupling, the phase quadrature increases (due to backaction), whereas the amplitude quadrature does not change. In contrast, in the case of pure dissipative coupling, the situation is the opposite—the amplitude quadrature increases and the phase one does not change. For a combination of dispersive and dissipative coupling, the situation is more complicated [the denominators in Eqs. (4.1) contain both dissipative P_m and dispersive Q_m coefficients]; however, the numerator a_{1a} in Eq. (4.1a) demonstrates the dependence on a_ϕ with the dissipative coefficient P_m , and the numerator $a_{1\phi}$ in Eq. (4.1b) depends on a_a with the dispersive coefficient Q_m .

It follows from Eqs. (4.1) that both quadratures are suitable for detecting the signal force. We use the homodyne detection for the measurement of quadratures as follows:

$$a_{1\theta} = a_{1a} \cos \theta + a_{1\phi} \sin \theta, \quad (4.3)$$

where θ is a homodyne angle. Let the input field be in the coherent state. This means that single-sided power spectral densities (PSD) of quadratures a_a and a_ϕ are equal: $S_a(\Omega) = S_\phi(\Omega) = 1$ [14]. Then the noise PSD recalculated to f_s can be easily derived from Eqs. (4.1):

$$S_f = S_{a1} + S_{\phi1}, \quad (4.4a)$$

$$S_{a1} = \frac{(x_0^2 - x^2 + Q_m D^2 \tan^2 \theta)^2}{2x^2(x^2 P_m + D^2 Q_m \tan^2 \theta)}, \quad (4.4b)$$

$$S_{\phi1} = \frac{[(x_0^2 - x^2) \tan \theta - P_m x^2]^2}{2x^2(x^2 P_m + D^2 Q_m \tan^2 \theta)}. \quad (4.4c)$$

Here the SQL sensitivity corresponds to $S_f = 1$. When $\theta = 0$ we measure the amplitude quadrature, and when $\theta = \frac{\pi}{2}$ we measure the phase quadrature.

Let us fix $x = x_c$ and find $\tan \theta$ at which Eqs. (4.4) takes an extreme value. There are two $\tan \theta$ angles and they have the

following forms:

$$\tan \theta_1 = -\frac{x_0^2 - x_c^2}{Q_m D^2}, \quad \tan \theta_2 = \frac{P_m x_c^2}{x_0^2 - x_c^2}. \quad (4.5)$$

Choosing these homodyne angles we completely cancel the noise determined by one of the quadratures, namely, $S_{a1}^{x=x_c} = 0$ at $\theta = \theta_1$ and $S_{\phi_1}^{x=x_c} = 0$ at $\theta = \theta_2$.

Let us consider a special case: $x_c = x_0$. Then $\tan \theta_1 = 0$ and $\tan \theta_2 = \pm\infty$. This means that we measure the quadrature of the amplitude or the phase. In these measurements PSDs have the following forms:

$$S_f|_{\theta=0} = \frac{1}{2} \left\{ P_m + \frac{[(\frac{x_0}{x})^2 - 1]^2}{P_m} \right\}, \quad (4.6a)$$

$$S_f|_{\theta=\frac{\pi}{2}} = \frac{1}{2x^2} \left[Q_m D^2 + \frac{(x_0^2 - x^2)^2}{Q_m D^2} \right]. \quad (4.6b)$$

In the resonance case $\Omega = \Omega_0$,

$$S_f(\Omega_0)|_{\theta=0} = \frac{P_m}{2} = x_0^2 g, \quad g = \sqrt{\frac{P_m}{Q_m D^2}}, \quad (4.7a)$$

$$S_f(\Omega_0)|_{\theta=\pi/2} = \frac{D^2 Q_m}{2x_0^2} = \frac{1}{g}. \quad (4.7b)$$

Here we rewrite the PSD using Eqs. (4.1c) and (4.1d); g is a ratio between coefficients of optomechanical couplings (optomechanical ratio).

The relations Eqs. (4.7) show that at a small optomechanical ratio of $g \ll 1/\sqrt{x_0}$ we have the inequality $S_f(\Omega_0)|_{\theta=0} \ll S_f(\Omega_0)|_{\theta=\pi/2}$ and in order to surpass the SQL near the resonant frequency we have to detect the amplitude quadrature (i.e., $\theta = 0$).

In the opposite case of a large optomechanical ratio of $g \gg 1/\sqrt{x_0}$ we have the inverse inequality $S_f(\Omega_0)|_{\theta=0} \gg S_f(\Omega_0)|_{\theta=\pi/2}$ and to surpass the SQL one has to detect the phase quadrature (i.e., $\theta = \pi/2$).

Recall that $S_f(\Omega_0)|_{\theta=0}$ and $S_f(\Omega_0)|_{\theta=\pi/2}$ are extremes of one function. The maximum (minimum) depends on the ratio g . However, for the special case of $g = 1/x_0$ they become equal to each other (the maximum and the minimum coincide):

$$S_f(\Omega_0)|_{\theta=0} = S_f(\Omega_0)|_{\theta=\pi/2} = x_0, \quad \text{at } g = \frac{1}{x_0}. \quad (4.8)$$

Thus, when $g = 1/x_0$ we get the same sensitivity near the resonant frequency for any quadrature detection. Usually $x_0 \ll 1$ (the case of the nonresolved sideband); hence, the SQL can be surpassed.

The minimum PSD is achieved at the resonant frequency and it is defined by Eqs. (4.7). This minimum PSD is realized inside a narrow bandwidth Γ :

$$\frac{\Gamma}{\Omega_0} \simeq S_f^{\min}. \quad (4.9)$$

Here Γ is defined as $S_f(\Omega_0 \pm \Gamma/2) \simeq 2S_f^{\min}$. The relation Eq. (4.9) corresponds to the known Cramer-Rao bound [47–49].

In Fig. 2 we depict graphs of the amplitude spectral densities $\sqrt{S_f(\Omega)}$ of noise recalculated to f_s by the homodyne

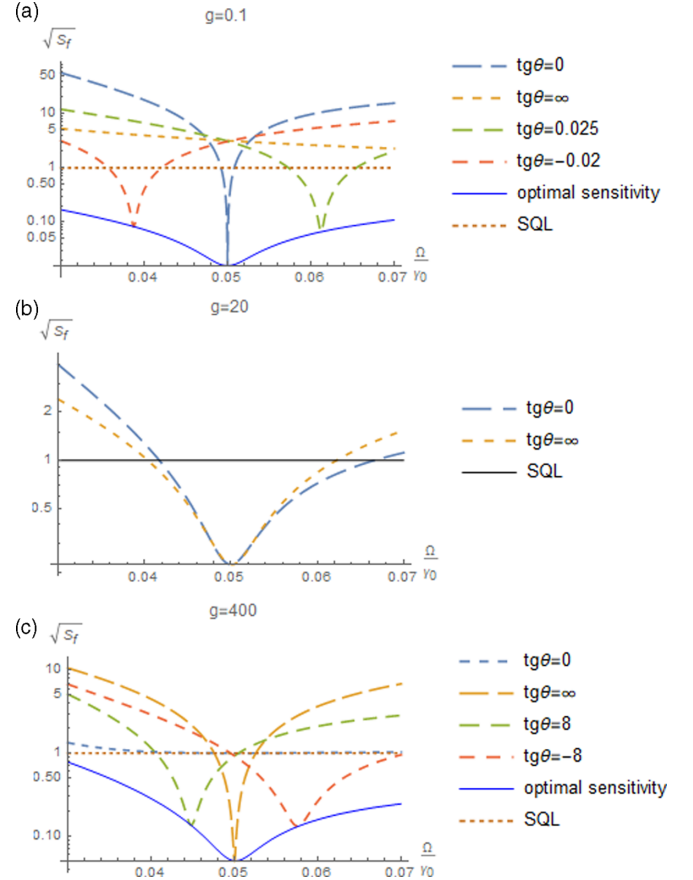


FIG. 2. Graphs of amplitude spectral densities $\sqrt{S_f(\Omega)}$ plotted for the homodyne detection having different homodyne angles and ratio g and fixed dimensionless frequency $x_0 = 0.05$. The graphs in panel (a) are obtained for $g = 0.1$. The graphs in panel (b) correspond to condition Eq. (4.8) $g = 1/x_0 = 20$. The graphs in panel (c) are plotted for the case $g = 400 \gg 1/x_0$. Also the graphs in panels (a) and (c) show the optimal PSD obtained at the optimal frequency-dependent homodyne angle (see Appendix B).

detection with different homodyne angles and ratio g and with fixed dimensionless frequency $x_0 = 0.05$ and pump power (so $|\xi \eta| = 1$). The main parameters (test mass, optical power) are taken from Table I with varying coupling ξ and η . The plots are given for preliminary chosen fixed homodyne angles. For methodical purposes in Figs. 2(a) and 2(c) we also show the optimal PSD by the optimal frequency-dependent homodyne angle (see Appendix B).

The graphs in Fig. 2(a) are obtained for $g = 0.1$. Varying the homodyne angle one can surpass the SQL at frequencies close to mechanical resonance. At mechanical resonance the sensitivity attains the minimum but in narrow bandwidth. The SQL can be surpassed when the frequency differs from the resonance one by about 50%, but the sensitivity will drop slightly and the bandwidth will be wider when compared to the case of mechanical resonance.

The graphs in Fig. 2(b) correspond to condition (4.8) $g = 1/x_0 = 20$. The SQL can be surpassed within a relatively wider bandwidth (about 50% of center frequency). Variation of the homodyne angle practically does not influence the sensitivity.

The graphs in Fig. 2(c) describe the case $g = 400 \gg 1/x_0$. Variation of the homodyne angle allows surpassing the SQL inside the bandwidths close to the mechanical resonance. It is similar to the case shown in Fig. 2(a).

Above we assumed that ξ and η can be varied *arbitrary*. But usually these coefficients are constant in certain systems. For example, the Fabry-Perot cavity with the MSI with the movable BS has fixed ξ and η [see Eq. (3.9)], and the ratio $g = T_0 \ll 1$.

If only the partially transmitting mirror M is movable in the MSI, then coefficients Eq. (3.11) are constant too, and $g = r_M/t_M$. In this case we can get an optomechanical system with a large coefficient g if $r_M \gg t_M$.

V. PONDEROMOTIVE SQUEEZING

We would like to pay attention to the fact that combined optomechanical coupling can also be used to produce a ponderomotive squeezed light. In turn, varying the ratio g Eq. (4.7a) between dispersive and dissipative coupling provides for a possibility to control output squeezing. The output quadrature Eq. (4.3) measured by the homodyne detector can be derived from Eqs. (4.1):

$$a_{1\theta} = \frac{(x_0^2 - x^2) \cos \theta + \frac{2x_0^2}{g} \sin \theta}{(x_0^2 - x^2) - 2ixx_0^2} a_a + \frac{(x_0^2 - x^2) \sin \theta - 2x_0^2 x^2 g \cos \theta}{(x_0^2 - x^2) - 2ixx_0^2} a_\phi. \quad (5.1)$$

In the case of the mechanical resonance $\Omega = \Omega_0$, this equation can be written as follows:

$$a_\theta|_{x=x_0} = \frac{i}{gx_0} \sin \theta a_a - ix_0 g \cos \theta a_\phi. \quad (5.2)$$

Obviously, in order to measure squeezing for small $g \ll 1/x_0$ one has to choose $\sin \theta = 0$ and to measure the amplitude output quadrature. In contrast, to measuring squeezing for large $g \gg 1/x_0$, one has to choose $\cos \theta = 0$ and to measure the phase output quadrature [see Eqs. (B1) in Appendix B]:

$$S_a(\Omega_0) = x_0^2 g^2 \quad (\sin \theta = 0), \quad (5.3a)$$

$$S_\phi(\Omega_0) = \frac{1}{g^2 x_0^2} \quad (\cos \theta = 0), \quad (5.3b)$$

where S_a and S_ϕ are single-sided PSDs of output amplitude and phase quadratures, respectively, and we assume that condition Eq. (4.2) is valid. Such squeezing near the resonant frequency Ω_0 is not observed in the case of dispersion coupling.

In case Eq. (4.8) $g = 1/x_0$, the output light is practically coherent and it is required to pay attention to scale on the vertical axis of the plots in Fig. 3(b).

Specifically, in the case of low frequencies $\Omega \ll \Omega_0$ ($x \ll x_0$), we get frequency-independent squeezing:

$$\Omega \ll \Omega_0, \quad g \ll 1: S_\theta^{\text{comb}} \simeq \frac{g^2}{4}, \quad (5.4)$$

where S_θ^{comb} is a single-sided PSD of the output quadrature Eq. (4.3) at the optimal homodyne angle in the case of combined coupling (see details in Appendix B).

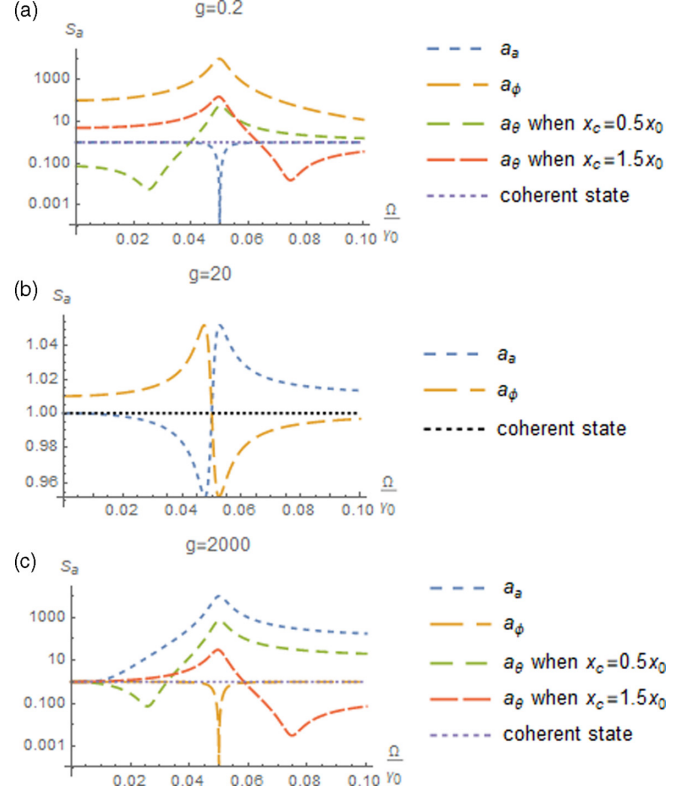


FIG. 3. Graphs of single-sided PSDs of different quadratures by different parameters g and the fixed resonant frequency $x_0 = 0.05$. The graphs in panel (a) are constructed for $g = 0.2 \ll 1/x_0$. The graphs in panel (b) are constructed for $g = 1/x_0 = 20$, and here we get an almost coherent state of the electromagnetic field (pay attention to scale on vertical axis). The graphs in panel (c) relate to the case $g = 2000 \gg 1/x_0$.

It is similar to what we obtained in the case of the dispersive coupling with a nonresonant pump ($\Delta = \omega_p - \omega_0$ is detuning) [46]:

$$\Omega \ll \Omega_0, \quad \frac{\Delta}{\gamma_0} \ll 1: S_\theta^{\text{disper}} \simeq \frac{\Delta^2}{\gamma_0^2}, \quad (5.5)$$

where S_θ^{disper} is a single-sided PSD of the output quadrature Eq. (4.3) at the optimal homodyne angle for dispersive coupling. The PSDs [Eqs. (5.4) and (5.5)] are equal to each other when $\frac{g}{2} = \frac{\Delta}{\gamma_0}$ and practically do not depend on the frequency.

In the general case we can adjust the maximum squeezing at the preliminary chosen dimensionless frequency x_c (near x_0) by varying the homodyne angle θ at a fixed ratio g (see details of calculations in Appendix B). If compared with the dispersive case the main advantage of combined coupling deals with the possibility to vary the degree of squeezing and its bandwidth by choosing x_c (i.e., the homodyne angle).

Shown in Fig. 3 are the plots of single-sided PSDs (B2c) obtained for the output light for the normalized mechanical frequency $x_0 = 0.05$ when $x_c = 0.5x_0$ or $x_c = 1.5x_0$ and different ratios g . For $g = 1/x_0$ [Fig. 3(b)], the output state is practically coherent at $\Omega = \Omega_0$ but out of resonance in the case of squeezing. But the farther g is from $1/x_0$, the stronger the squeezing becomes near x_0 . For small $g \ll 1/x_0$ we get

the amplitude quadrature squeezed near the resonance, and for large $g \gg 1/x_0$ we get the phase quadrature. It is possible to get less strong squeezing but in a wider frequency band at other frequencies. This can be done measuring a quadrature $a_{1\theta}$ other than the amplitude and the phase.

The combined coupling provides the possibility to produce frequency-dependent squeezing, which is often needed in precision optomechanical experiments. For example, in gravitational wave detectors injection of such squeezed light into the dark port allows one to increase sensitivity.

VI. DISCUSSION AND CONCLUSION

We analyzed the optomechanical system, featuring the combination of dispersive and dissipative coupling, and showed that the main properties of combined coupling deal with the optical rigidity Eqs. (2.9), which appears as a result of *both* kinds of coupling. At the same time, this rigidity manifests in systems having combined coupling on the resonant pump, which is not typical for pure dispersive [46] or dissipative [40] coupling types.

To realize the combination of dissipative and dispersive coupling we used the MSI as an input mirror in the FP cavity (see Fig. 1). We considered two different modes of operation of the MSI with a movable beam splitter and an immobile completely reflecting mirror M and vice versa with a movable partially transmitting mirror M and a fixed beam splitter. The coefficients of the dispersive ξ and the dissipative η coupling for these schemes were obtained. In further analysis, we assumed that ξ and η can be varied arbitrarily.

We considered an optomechanical system with a combination of both couplings as a signal force detector. Homodyne detection of an output field can have a sensitivity better than that of the SQL near the resonant frequency Ω_0 , which is defined by the optical rigidity Eq. (2.9d). The analysis shows that it is most effective to measure the amplitude or phase quadrature [the choice of the quadrature depends on the ratio g as compared with $1/x_0$ Eq. (4.8)]. If $g < 1/x_0$, it is better to measure the amplitude quadrature, and if $g > 1/x_0$, it is better to measure the phase quadrature. At $g = 1/x_0$, we get the same sensitivity near the resonant frequency for measuring *any* quadrature. In this case the PSD recalculated to force the SQL Eq. (4.8) is smaller than unity (i.e., the SQL can be surpassed) if $x_0 = \Omega_0/\gamma_0 \ll 1$.

The physical reason is related to the correlation between the measurement noise and the fluctuation backaction. This correlation occurs due to the combination of both optomechanical couplings. Indeed, the fluctuation backaction force Eq. (2.9b) depends on the phase quadrature (dissipative coupling) and on the amplitude quadrature (dispersive coupling), and the measurement noise is determined by the amplitude or phase quadrature [first terms in Eqs. (2.8a) and (2.8b)]. Part of the total noise is completely compensated at the resonant frequency [see Eqs. (4.1)]. The remaining noise recalculated to f_s is proportional to $\sqrt{P_m}$ or $\sqrt{D^2 Q_m/x_0}$, depending on which quadrature we measure. The SQL is surpassed if this noise is small.

We would like to point out that variation of ratio g between dispersive and dissipative coupling and choice of homodyne angle provides the possibility to control output ponderomotive

squeezing. Varying the homodyne angle we can obtain constant squeezing at frequencies much smaller than the resonant frequency Ω_0 , or large squeezing in the finite bandwidth (the larger the squeezing, the more narrow the bandwidth) near the resonant frequency. The ponderomotive squeezing induced by combined coupling has a wider range of varying squeezing parameters as compared with ponderomotive squeezing caused by dispersive coupling.

The combined coupling looks promising to be used in gravitational wave antennas for the creation of frequency-dependent squeezing with controllable parameters. The main obstacle is thermal mechanical noise. It is the subject of our future research.

ACKNOWLEDGMENTS

The authors are grateful to Haixing Miao for fruitful discussion and advice. They are grateful for support provided by the Russian Foundation for Basic Research (Grant No. 19-29-11003), the Interdisciplinary Scientific and Educational School of M.V. Lomonosov Moscow State University “Fundamental and Applied Space Research,” and for TAPIR GIFT MSU Support from the California Institute of Technology.

APPENDIX A: INTRACAVITY AND OUTSIDE FIELDS

From the Hamiltonian Eqs. (2.1) we obtain the following set of equations describing the time evolution of the optomechanical system:

$$\dot{\hat{a}}_c = -i\omega_0(1 + \xi\hat{y})\hat{a}_c - \sqrt{\gamma} \int_0^\infty \hat{b}_\omega \frac{d\omega}{2\pi}, \quad (\text{A1a})$$

$$\dot{\hat{b}}_\omega = -i\omega\hat{b}_\omega + \sqrt{\gamma}\hat{a}_c,$$

$$\ddot{\hat{y}} = -\frac{\hbar\omega_0\xi}{m}\hat{a}_c^\dagger\hat{a}_c + \frac{F_s}{m} - i\frac{\sqrt{\gamma_0}\eta\hbar}{2m} \int_0^\infty (\hat{b}_\omega\hat{a}_c^\dagger - \hat{a}_c\hat{b}_\omega^\dagger) \frac{d\omega}{2\pi}. \quad (\text{A1b})$$

We present the annihilation operators of the input and intracavity optical field through slow amplitudes as

$$\hat{a}_c(t) \Rightarrow \hat{a}_c(t)e^{-i\omega_0 t}, \quad \hat{b}_\omega(t) \Rightarrow \hat{b}_\omega(t)e^{-i\omega t}. \quad (\text{A2})$$

The differential equations for these slow amplitudes have the following forms:

$$\dot{\hat{a}}_c = -i\omega_0\xi\hat{y}\hat{a}_c - \sqrt{\gamma} \int_0^\infty \hat{b}_\omega e^{i(\omega_0-\omega)t} \frac{d\omega}{2\pi}, \quad (\text{A3a})$$

$$\dot{\hat{b}}_\omega = \sqrt{\gamma}\hat{a}_c e^{i(\omega-\omega_0)t}. \quad (\text{A3b})$$

The solution for \hat{b}_ω can be written in two ways, in terms of initial conditions at time $t > t_0$ (input) or in terms of final conditions $t < t_1$ (output):

$$\hat{b}_\omega(t) = \hat{b}_\omega(t_0) + \sqrt{\gamma} \int_{t_0}^t \hat{a}_c(t') e^{-i(\omega_0-\omega)t'} dt', \quad (\text{A4a})$$

$$\hat{b}_\omega(t) = \hat{b}_\omega(t_1) - \sqrt{\gamma} \int_t^{t_1} \hat{a}_c(t') e^{-i(\omega_0-\omega)t'} dt'. \quad (\text{A4b})$$

Let us substitute the resulting expressions in Eqs. (A3) and represent the frequency ω as the sum $\omega = \omega_0 + \Omega$, where ω_0 is the frequency of the light wave, and Ω is the frequency of

the signal force F_s . It is several orders of magnitude less than the frequency of the electromagnetic wave $\omega_0 \simeq 10^{15}$ Hz, so in Eqs. (A3), instead of integrating from $-\omega_0$, we formally integrate from $-\infty$:

$$\hat{a}_c = -i\omega_0\xi\hat{y}\hat{a}_c + \sqrt{\gamma}\hat{a}_{\text{in}} - \frac{\gamma}{2}\hat{a}_c, \quad (\text{A5a})$$

$$\hat{a}_c = -i\omega_0\xi\hat{y}\hat{a}_c - \sqrt{\gamma}\hat{a}_{\text{out}} + \frac{\gamma}{2}\hat{a}_c, \quad (\text{A5b})$$

$$\hat{a}_{\text{in}} = -\int_{-\infty}^{\infty} \hat{b}_\omega(t_0)e^{-i\Omega t} \frac{d\Omega}{2\pi}, \quad (\text{A5c})$$

$$\hat{a}_{\text{out}} = \int_{-\infty}^{\infty} \hat{b}_\omega(t_1)e^{-i\Omega t} \frac{d\Omega}{2\pi}. \quad (\text{A5d})$$

The minus sign in Eq. (A5c) is a phase convention: left-going fields are negative, and right-going fields are positive.

This expression shows how the input and output fields are related:

$$\hat{a}_{\text{in}} + \hat{a}_{\text{out}} = \sqrt{\gamma}\hat{a}_c. \quad (\text{A6})$$

The equation of motion in this case will have the following form:

$$\ddot{y} = -\frac{\hbar\omega_0\xi}{m}\hat{a}_c^\dagger\hat{a}_c + \frac{F_s}{m} - i\frac{\sqrt{\gamma_0}\eta\hbar}{2m}(\hat{a}_{\text{in}}\hat{a}_c^\dagger - \hat{a}_c\hat{a}_{\text{in}}^\dagger). \quad (\text{A7})$$

Let us express slow amplitudes as large constant amplitudes (denoted by capital letters) plus small amplitudes (denoted by the same letters in lowercase) to describe the noise and signal components:

$$\hat{a}_c = A_0 + \hat{a}_0, \quad \hat{a}_{\text{in}} = A + \hat{a}, \quad \hat{a}_{\text{out}} = A_1 + \hat{a}_1. \quad (\text{A8})$$

Let us apply the Fourier transform to Eqs. (A5). The Fourier transform can be defined as follows:

$$\hat{a}(t) = \int_{-\infty}^{\infty} a(\Omega)e^{-i\Omega t} \frac{d\Omega}{2\pi}, \quad (\text{A9})$$

and similarly for other values denoting the Fourier transform by the same letter without a hat.

We assume that in Eq. (A8) the expected values exceed the fluctuation parts of the operators. So we make use of the method of successive approximation to derive a set of equations describing the system. We select $A_0 = A_0^*$ and find the following in the zero-order approximation:

$$A_1 = A, \quad A_0 = \frac{2}{\sqrt{\gamma_0}}A. \quad (\text{A10})$$

One can find equations for the fluctuation part of the field and the displacement of the test mass in the first-order approximation. In the spectral representation they have the following form:

$$a_0(\Omega) = \frac{\sqrt{\gamma_0}}{\frac{\gamma_0}{2} - i\Omega}a(\Omega) - \left(\frac{\sqrt{\gamma_0}\eta A}{2(\frac{\gamma_0}{2} - i\Omega)} + \frac{2i\omega_0\xi A}{\sqrt{\gamma_0}(\frac{\gamma_0}{2} - i\Omega)} \right)y_\Omega, \quad (\text{A11a})$$

$$a_1(\Omega) = \frac{\frac{\gamma_0}{2} + i\Omega}{\frac{\gamma_0}{2} - i\Omega}a(\Omega) - \left(\frac{i\Omega\eta A}{\frac{\gamma_0}{2} - i\Omega} + \frac{i2\omega_0\xi A}{\frac{\gamma_0}{2} - i\Omega} \right)y_\Omega, \quad (\text{A11b})$$

$$y_\Omega = -\frac{F_\Omega}{m\Omega^2} + \frac{\hbar\omega_0\xi}{m\Omega^2}A_0[a_0(\Omega) + a_0^\dagger(-\Omega)] + i\frac{\sqrt{\gamma_0}\eta\hbar}{2m\Omega^2}\{A[a_0^\dagger(-\Omega) - a_0(\Omega)] + A_0[a(\Omega) - a^\dagger(-\Omega)]\}. \quad (\text{A11c})$$

Here y_Ω and F_Ω are Fourier transforms of the displacement y and the signal F_s , respectively.

APPENDIX B: THE ANALYSIS OF THE PONDERMOTIVE SQUEEZING

From Eq. (5.1) one can calculate the single-sided PSD assuming coherent input light as follows:

$$S_\theta = \frac{(x_0^2 - x^2)^2 + 4x_0^4\left(\frac{\sin^2\theta}{g^2} + x^4g^2\cos^2\theta\right)}{(x_0^2 - x^2)^2 + 4x^2x_0^4} + \frac{4x_0^2(x_0^2 - x^2)\sin\theta\cos\theta\left(\frac{1}{g} - x^2g\right)}{(x_0^2 - x^2)^2 + 4x^2x_0^4} = \frac{W + U\cos 2\theta + V\sin 2\theta}{(x_0^2 - x^2)^2 + 4x^2x_0^4} \quad (\text{B1a})$$

$$W = (x_0^2 - x^2)^2 + \frac{2x_0^4}{g^2} + 2x^4x_0^4g^2, \quad (\text{B1b})$$

$$U = 2x_0^2\left[x^4x_0^2g^2 - \frac{x_0^2}{g^2}\right], \quad (\text{B1c})$$

$$V = 2x_0^2(x_0^2 - x^2)\left[\frac{1}{g} - x^2g\right]. \quad (\text{B1d})$$

The minimum of S_θ at $x = x_c$ takes place at the homodyne angle θ defined as

$$\cos 2\theta = -\frac{U_c}{\sqrt{U_c^2 + V_c^2}}, \quad \sin 2\theta = -\frac{V_c}{\sqrt{U_c^2 + V_c^2}}, \quad (\text{B2a})$$

$$U_c = U|_{x=x_c}, \quad V_c = V|_{x=x_c}. \quad (\text{B2b})$$

and it is equal to

$$S_\theta^{x_c}(x) = \frac{W - \frac{UU_c + VV_c}{\sqrt{U_c^2 + V_c^2}}}{(x_0^2 - x^2)^2 + 4x^2x_0^4}. \quad (\text{B2c})$$

In the particular case $x \ll x_0$, we have

$$W \simeq x_0^4\left(1 + \frac{2}{g^2}\right), \quad U \simeq -\frac{2x_0^4}{g^2}, \quad V \simeq \frac{2x_0^4}{g}, \quad (\text{B3a})$$

$$S_\theta^{x \ll x_0} \simeq 1 + \frac{2}{g^2} - \frac{2}{g^2}\cos 2\theta + \frac{2}{g}\sin 2\theta \geq \frac{\sqrt{1+g^2}-1}{\sqrt{1+g^2+1}} = \frac{g^2}{4} - \frac{g^4}{8} + \dots \quad (\text{B3b})$$

- [1] (LVC Collaboration), Prospects for observing and localizing gravitational-wave transients with Advanced LIGO and Advanced Virgo, *Living Rev. Relativ.* **23**, 3 (2020).
- [2] J. Aasi *et al.* (LIGO Scientific Collaboration), Advanced LIGO, *Classical Quantum Gravity* **32**, 074001 (2015).
- [3] D. Martynov *et al.*, Sensitivity of the Advanced LIGO detectors at the beginning of gravitational wave astronomy, *Phys. Rev. D* **93**, 112004 (2016).
- [4] F. Acernese *et al.*, Advanced Virgo: a 2nd generation interferometric gravitational wave detector, *Classical Quantum Gravity* **32**, 024001 (2015).
- [5] K. L. Dooley, J. R. Leong, T. Adams, C. Affeldt, A. Bisht, C. Bogan, J. Degallaix, C. Graf, S. Hild, and J. Hough, GEO 600 and the GEO-HF upgrade program: successes and challenges, *Classical Quantum Gravity* **33**, 075009 (2016).
- [6] Y. Aso, Y. Michimura, K. Somiya, M. Ando, O. Miyakawa, T. Sekiguchi, D. Tatsumi, and H. Yamamoto, Interferometer design of the KAGRA gravitational wave detector, *Phys. Rev. D* **88**, 043007 (2013).
- [7] S. Forstner, S. Prams, J. Knittel, E. D. van Ooijen, J. D. Swaim, G. I. Harris, A. Szorkovszky, W. P. Bowen, and H. Rubinsztein-Dunlop, Cavity Optomechanical Magnetometer, *Phys. Rev. Lett.* **108**, 120801 (2012).
- [8] B.-B. Li, J. Břílek, U. Hoff, L. Madsen, S. Forstner, V. Prakash, C. Schafermeier, T. Gehring, W. Bowen, and U. Andersen, Quantum enhanced optomechanical magnetometry, *Optica* **5**, 850 (2018).
- [9] M. Wu, A. C. Hryciw, C. Healey, D. P. Lake, H. Jayakumar, M. R. Freeman, J. P. Davis, and P. E. Barclay, Dissipative and Dispersive Optomechanics in a Nanocavity Torque Sensor, *Phys. Rev. X* **4**, 021052 (2014).
- [10] P. H. Kim, B. D. Hauer, C. Doolin, F. Souris, and J. P. Davis, Approaching the standard quantum limit of mechanical torque sensing, *Nat. Commun.* **7**, 13165 (2016).
- [11] J. Ahn, Z. Xu, J. Bang, P. Ju, X. Gao, and T. Li, Ultrasensitive torque detection with an optically levitated nanorotor, *Nat. Nanotechnol.* **15**, 89 (2020).
- [12] V. B. Braginsky, Classic and quantum limits for detection of weak force on acting on macroscopic oscillator, *Sov. Phys. JETP* **26**, 831 (1968).
- [13] V. B. Braginsky and F. Ya. Khalili, *Quantum Measurement* (Cambridge University, Cambridge, England, 1992).
- [14] H. J. Kimble, Y. Levin, A. B. Matsko, K. S. Thorne, and S. P. Vyatchanin, Conversion of conventional gravitational-wave interferometers into QND interferometers by modifying input and/or output optics, *Phys. Rev. D* **65**, 022002 (2001).
- [15] T. Kippenberg and K. Vahala, Cavity optomechanics: Back action at the mesoscale, *Science* **321**, 1172 (2008).
- [16] J. M. Dobrindt and T. J. Kippenberg, Theoretical Analysis of Mechanical Displacement Measurement Using a Multiple Cavity Mode Transducer, *Phys. Rev. Lett.* **104**, 033901 (2010).
- [17] S. P. Vyatchanin and A. B. Matsko, Quantum limit of force measurement, *Sov. Phys. JETP* **77**, 218 (1993).
- [18] S. Vyatchanin and E. Zubova, Quantum variation measurement of force, *Phys. Lett. A* **201**, 269 (1995).
- [19] LIGO Scientific Collaboration, A gravitational wave observatory operating beyond the quantum shot-noise limit, *Nat. Phys.* **7**, 962 (2011).
- [20] LIGO Scientific Collaboration and Virgo Collaboration, Enhanced sensitivity of the LIGO gravitational wave detector by using squeezed states of light, *Nat. Photonics* **7**, 613 (2013).
- [21] V. Tse *et al.*, Quantum-Enhanced Advanced LIGO Detectors in the Era of Gravitational-Wave Astronomy, *Phys. Rev. Lett.* **123**, 231107 (2019).
- [22] F. Acernese *et al.* (Virgo Collaboration), Increasing the Astrophysical Reach of the Advanced Virgo Detector via the Application of Squeezed Vacuum States of Light, *Phys. Rev. Lett.* **123**, 231108 (2019).
- [23] M. Yap *et al.*, Broadband reduction of quantum radiation pressure noise via squeezed light injection, *Nat. Photonics* **14**, 19 (2020).
- [24] H. Yu *et al.*, Quantum correlations between the light and kilogram-mass mirrors of LIGO, *Nature (London)* **583**, 43 (2020).
- [25] J. Cripe *et al.*, Measurement of quantum back action in the audio band at room temperature, *Nature (London)* **568**, 364 (2019).
- [26] V. B. Braginsky and F. Ya. Khalili, Gravitational wave antenna with QND speed meter, *Phys. Lett. A* **147**, 251 (1990).
- [27] V. B. Braginsky, M. L. Gorodetsky, F. Y. Khalili, and K. S. Thorne, Dual-resonator speed meter for a free test mass, *Phys. Rev. D* **61**, 044002 (2000).
- [28] V. B. Braginsky and F. Ya. Khalili, Low noise rigidity in quantum measurements, *Phys. Lett. A* **257**, 241 (1999).
- [29] F. Ya. Khalili, Frequency-dependent rigidity in large-scale interferometric gravitational-wave detectors, *Phys. Lett. A* **288**, 251 (2001).
- [30] M. Tsang and C. M. Caves, Coherent Quantum-Noise Cancellation for Optomechanical Sensors, *Phys. Rev. Lett.* **105**, 123601 (2010).
- [31] E. Polzik and K. Hammerer, Trajectories without quantum uncertainties, *Ann. Phys.* **527**, A15 (2015).
- [32] C. B. Møller, R. Thomas, G. Vasilakis, E. Zeuthen, Y. Tsaturyan, M. Balabas, K. Jensen, A. Schliesser, K. Hammerer, and E. Polzik, Quantum back-action-evading measurement of motion in a negative mass reference frame, *Nature (London)* **547**, 191 (2017).
- [33] F. Elste and S. M. Girvin, and A. A. Clerk, Quantum Noise Interference and Backaction Cooling in Cavity Nanomechanics, *Phys. Rev. Lett.* **102**, 207209 (2009).
- [34] M. Li, W. H. P. Pernice, and H. X. Tang, Reactive Cavity Optical Force on Microdisk-Coupled Nanomechanical Beam Waveguides, *Phys. Rev. Lett.* **103**, 223901 (2009).
- [35] T. Weiss, C. Bruder, and A. Nunnenkamp, Strong-coupling effects in dissipatively coupled optomechanical systems, *New J. Phys.* **15**, 045017 (2013).
- [36] A. Hryciw, M. Wu, B. Khanaliloo, and P. Barclay, Tuning of nanocavity optomechanical coupling using a near-field fiber probe, *Optica* **2**, 491 (2015).
- [37] A. Xuereb, R. Schnabel, and K. Hammerer, Dissipative Optomechanics in a Michelson-Sagnac Interferometer, *Phys. Rev. Lett.* **107**, 213604 (2011).
- [38] S. P. Tarabrin, H. Kaufer, F. Y. Khalili, R. Schnabel, and K. Hammerer, Anomalous dynamic backaction in interferometers, *Phys. Rev. A* **88**, 023809 (2013).
- [39] A. Sawadsky, H. Kaufer, R. M. Nia, S. P. Tarabrin, F. Y. Khalili, K. Hammerer, and R. Schnabel, Observation of Generalized Optomechanical Coupling and Cooling on Cavity Resonance, *Phys. Rev. Lett.* **114**, 043601 (2015).

- [40] S. P. Vyatchanin and A. B. Matsko, Quantum speed meter based on dissipative coupling, *Phys. Rev. A* **93**, 063817 (2016).
- [41] A. Nazmiev and S. Vyatchanin, Stable optical rigidity based on dissipative coupling, *J. Phys. B: At., Mol. Opt. Phys.* **52**, 155401 (2019).
- [42] A. Karpenko and S. P. Vyatchanin, Dissipative coupling, dispersive coupling, and their combination in cavityless optomechanical systems, *Phys. Rev. A* **102**, 023513 (2020).
- [43] S. Huang and G. S. Agarwal, Reactive-coupling-induced normal mode splittings in microdisk resonators coupled to waveguides, *Phys. Rev. A* **81**, 053810 (2010).
- [44] S. Huang and G. S. Agarwal, Reactive coupling can beat the motional quantum limit of nanowaveguides coupled to a microdisk resonator, *Phys. Rev. A* **82**, 033811 (2010).
- [45] D. Walls and G. Milburn, *Quantum Optics* (Springer-Verlag, Berlin, 2008).
- [46] T. Corbitt, Y. Chen, F. Khalili, D. Ottoway, S. Vyatchanin, S. Whitcomb, and N. Mavalvala, Squeezed-state source using radiation-pressure-induced rigidity, *Phys. Rev. A* **73**, 023801 (2006).
- [47] J. Mizuno, Comparison of optical configurations for laser-interferometric gravitational-wave detectors, Ph.D. thesis, Hannover University, 1995.
- [48] J. Mizuno, K. Strain, P. Nelson, J. Chen, R. Schilling, A. Rüdiger, W. Winkler, and K. Danzmann, Resonant sideband extraction: a new configuration for interferometric gravitational wave detectors, *Phys. Lett. A* **175**, 273 (1993).
- [49] H. Miao, R. X. Adhikari, Y. Ma, B. Pang, and Y. Chen, Towards the Fundamental Quantum Limit of Linear Measurements of Classical Signals, *Phys. Rev. Lett.* **119**, 050801 (2017).